Int. J. Electrochem. Sci., 12 **(2017)** 6545 – 6556, doi: 10.20964/2017.07.78

International Journal of
ELECTROCHEMICAL
SCIENCE
www.electrochemsci.org

Fabrication of N-doped Carbon Derived from poly(acrylonitrile)-ionic Liquid Copolymer and Application in Lithium Ion Batteries

Lei Wang[1], *Fuliang Zhu*[1], *Jun Xia*[1], *Gongrui Wang*[1], *Yanshuang Meng*[1,3,*], *Yue Zhang*[2,*]

[1] School of Materials Science and Engineering, Lanzhou University of Technology, Lanzhou 730050, China
[2] Department of Mechanical and Industrial Engineering, Texas A&M University-Kingsville, Kingsville, Texas, 78363, USA
[3] State Key Laboratory of Advanced Processing and Recycling of Non-ferrous Metals, Lanzhou 730050, China
[*]E-mail address: mengyanshuang@163.com, yue.zhang@tamuk.edu

Received: 12 April 2017 / *Accepted:* 19 May 2017 / *Published:* 12 June 2017

Nitrogen-doped carbon materials have been prepared by soap-free emulsion with poly(acrylonitrile) (PAN) and poly(acrylonitrile)-ionic liquid copolymer (PAN-PIL) as carbon sources. The carbonized PAN-PIL (CPAN-PIL) shows a higher nitrogen content (6.80 at.%.) than the carbonized PAN (CPAN) (2.32 at.%). The ionic liquid copolymer introduced graphitic nitrogen to CPAN-PIL, which was not observed in CPAN. The high nitrogen content and graphic nitrogen improved the electrical conductivity and increased the number of active sites. Therefore, CPAN-PIL displayed a specific capacity of 381 mAh g^{-1} after 50 cycles, which is 23% higher than the specific capacity of CPAN.

Keywords: Poly(acrylonitrile)-ionic liquid copolymer; N-doped carbon; Lithium ion batteries

1. INTRODUCTION

LIBs are one of the most promising energy storage technologies for applications in the field of portable electronics as wells as electronic vehicles, because of their many beneficial properties such as long cycling life, no memory effect, high energy density and high electrical conductivity [1-4]. Numerous studies revealed that the performance of LIBs is largely determined by the electrode materials, especially the anode materials [5, 6]. Carbon base-based materials, such as graphite, are the commonly used materials to form LIBs electrode due to their high electrical conductivity, excellent

cyclic stability and low price[7-9]. However, the shortcomings of traditional graphite, such as low theoretical specific capacity (372mAh g^{-1}), poor cycling performance at high current and low potential of Li-insertion, could cause the growth of lithium dendrite and short-circuit [10, 11]. Therefore, graphite anode cannot meet the increasing requirement of high-power LIBs for large-scale electronic vehicles. Hence, many other carbonaceous materials were studied as anode material for LIBs, including carbon nanotube, graphene, porous carbon and amorphous carbon[12, 13]. Among all these carbonaceous materials, amorphous carbon possesses higher capacity than graphite due to its abundant lattice defects and low degree of graphitization, which can generate adequate sites for Li^+ insertion[14, 15]. To address these intrinsic drawbacks existed in graphite anode material, many method have been investigated, including surface modification of carbonaceous materials[16, 17], recombination with other materials[18, 19] and doping with heteroatom (B, P, N or S) [20-23]. Among these methods , doping with heteroatom has been investigated to a lesser extend but is gaining increased interest since the integration of heteroatom in the carbon framework can effectively enhance the electrode/electrolyte wettability, the reactivity and the electrical conductivity, which lead to improved electrochemical performance. Recently, nitrogen has become the focus of doped heteroatom because of its high electronegativity (3.5 V) and low atomic volume, which can extend the capacity and the rate performance of carbonaceous materials[12, 24]. Nitrogen dopant can lower the valence band in carbon materials and enhance the electron density of Fermi level, making the material more stable [25]. Additionally, the high electron density of the Fermi level can significantly strengthen the electron donor states and increase the number of active sites, which can greatly improve the kinetics of Li^+ diffusion and transfer.

The doped nitrogen atoms exist in carbon frame in two forms: chemical nitrogen and structural nitrogen. The chemical nitrogen exists in chemical groups, like nitrosyl groups, and can be introduced to carbon frame by heating nitrogen source such as ammonia or nitric acid[26, 27]. The structural nitrogen, such as pyridinic-N, pyrrolic-N, and graphitic-N, is grafted to the skeletons of carbon materials by *in-situ* doping with nitrogen-rich sources[28]. It is worth mentioning that the graphitic-N can be ionized to liberate its electrons and form an electron-rich structure of carbon matrix, which can increase the electrical conductivity of carbon materials[29]. The commonly used nitrogen sources for *in-situ* doping can be generally divided into two groups: (1) biomaterials, like chitosan[30, 31], garlic peel[32], and honeysuckle[33]; (2) nitrogen-containing polymers or organic compounds such as polypyrrole[34, 35], melamine[36] and polyacrylonitrile (PAN)[37, 38]. Among all of these nitrogen sources, PAN is attracting more research interest because of many of its excellent properties such as high nitrogen content, high carbon residue rate and outstanding thermal stability [39, 40]. Moreover, PAN can be used to produce carbon materials of various structures, such as microspheres, fibers and nanofibers[41].

In recent years, there have been a large number of publications in the applications of ionic liquid (IL) for LIBs and their popularity has led to an increased interest in similarly structured materials, such as nitrogen-rich poly(ionic liquids) (PILs) [42]. PILs are one of the most promising carbon sources for electrode materials in LIBs due to their designable structure and high carbon residue rate. Balach et al. fabricated nitrogen-doped hollow carbon sphere carbonized from PILs , which exhibited excellent reversible capacity and high coulombic efficiency due to the tunable

nitrogen content and wall thickness of the carbonaceous material [43]. Yuan et al. successfully prepared nitrogen-doped carbon capsules with 7 wt.% nitrogen from PILs[44]. In spite of numerous efforts on exploring the suitable materials for preparing nitrogen doped carbon materials, there are very few studies that investigate how the nitrogen-rich precursors affect the electrochemical properties of nitrogen doped carbon materials.

In our previous work, we prepared nitrogen-doped carbon by microwave-assisted pyrolysis of ionic liquid[45]. The doped nitrogen atoms created a porous structure and a large number of active sites for the Li^+ ion adsorption, thus delivering high electrochemical performances. In this work, we have designed a simple way to fabricate nitrogen doped amorphous carbon particles with different nitrogen contents by carbonizing PAN and PAN-PIL, respectively. It is found that the IL has a great influence on the morphology, the form of the doped nitrogen-, which significantly affect the reversible capacity, coulombic efficiency and cycle performance of the obtained carbon particles. The carbonized PAN-PIL (CPAN-PIL) material exhibits a higher specific capacity and rate performance than the carbonized PAN (CPAN).

2. EXPERIMENTAL

2.1 Materials

The IL 1-vinyl-3-ethylimidazolium tetrafluoroborate ([VEIm]BF_4) was purchased from Lanzhou Institute of Chemical Physics and acrylonitrile (AN) from Kaixin chemical co., Ltd (Tianjin, China), which were the monomers for our research. The initiator 2,2-azobis (2-isobutyronitrile) (AIBN) was supplied by Sinopharm Chemical Regent Co., Ltd (Shanghai, PR China). Poly(ethylene glycol) diacrylate (PEGDA) and N-methyl-2-pyrrolidone (NMP) were obtained from Aladdin (China) and used as the crosslinker . The electrolyte was obtained from Beijing Institute of Chemical Reagent (Beijing, China). The Celgard membrance (Celgard 2400) with a thickness of 20μm was supplied by Shanxi Power Battery Material Co., Ltd (Shanxi, China). Ethanol absolute was purchased from Guanghua Sci-Tech Co., Ltd (Guangdong, China). The distilled water was made by the Ultrapure Water Polishing System when the resistivity under 18MΩ $\cdot cm^{-1}$. The 2032 type button cell, stainless steel spacers, copper foil, Li metal foils and polyvinylidenefluoride (PVDF) all purchased from Kejing Wisdom of Sci-Tech Co., Ltd (Shenzhen, China). All the agents were analytical grade and used no any further treatment.

2.2 Preparation of PAN and PAN-PIL

PAN and PAN-PIL were synthesized by soap-free emulsion. First, the mixed solution of 40ml ethanol absolute and 44ml distilled water (in a weight ratio of 1: 1.4) as solvent, AIBN as initiators were dissolved in 11.2g AN and poured into a 150 ml three-neck round-bottom flask with the solvent. Then add 2.0g PEGDA into the flask. The reaction device was equipped with a condenser pipe and heated in water bath kettle at 65ºC with tempestuously stirring under nitrogen atmosphere for 15 h.

The PAN powder were obtain by suction filtration and washed with ethanol absolute to remove the residual initiators and crosslinker. Then the PAN particles were dried at 80 ºC for 24 h in a vacuum drying oven. PAN-PIL was obtained by the above method except the monomers were blended by 1.7g [VEIm]BF_4 and 9.5g AN (in a weight ratio of 15:85).

2.3 Pyrolysis of PAN and PAN-PIL particles

The carbonization process of PAN and PAN-PIL was divided into two stages. Firstly, certain amount of the dried PAN or PAN-PIL powders was put into the crucible. Then the samples were heated at 250 ºC for 4 h in a muffle furnace at air atmosphere with the heating rate of 5 ºC min^{-1}. Secondly, the samples were carbonized in the tube furnace at 900 ºC for 2h under N_2 atmosphere and with a same heating rate of 5ºC min^{-1}. The final products were denoted as CPAN and CPAN-PIL, respectively.

2.4 Material Characterization

The morphologies of CPAN and CPAN-PIL were obtained by Quanta 450FEG field emission scanning electron microscope (SEM) handled under the acceleration voltage of 20kV. The X-ray powder diffraction (XRD) patterns of CPAN and CPAN-PIL were gained on D/max-2400 diffraction system with a range of 2-theta 10º-80º(Cu-Kα, λ=0.15406 nm). The thermogravimetric analysis and differential scanning calorimetry (TG/DSC) of PAN and PAN-PIL were measured by the DSC 200F3 thermal analyzer at a heating rate of 10 ºCmin^{-1} under N_2 atmosphere. The temperature interval was from 20ºC to 1000ºC. X-ray Photoelectron pectroscopic (XPS) patterns of CPAN and CPAN-PIL were obtained by ESCALAB 250Xi equipped with a aluminum target X-ray source(Al- Kα,1486.6ev).

2.5 Electrochemical Measurements

To investigate the electrochemical performances of CPAN and CPAN-PIL as anode materials for LIBs, CR2032 type half cells were assembled in an argon-filled glove box. The working electrodes were made from CPAN or CPAN-PIL materials, acetylene black and polyvinylidenefluoride (PVDF) in the mass ratio of 8:1:1. The above materials and N-methyl-2-pyrrolidone (NMP) were ground into the fine and smooth slurry. Then the slurry was coated on the copper foil uniformly and dried in vacuum for 12h at 80 ºC. The Celgard membrance (Celgard 2400) were employed as a separator and Li metal foils as counter electrode. The electrolyte solution was composed of 1M $LiPF_6$ and a mixture of ethylene carbonate and 1,2-dimethoxyethane with equal volume proportion. The batteries were tested after 24 hours standing. The galvanostatic method charge/discharge measurement was tested by LAND CT2001A equipment in the voltage range of 0.005~3.0V. The cyclic voltammetry (CV) curves were tested by CHI 660D electrochemical workstation with a scanning rate of 0.1mV s^{-1} in the voltage range of 0.005~3.0V. The electrochemical spectroscopy (EIS) was measured in the same equipment within the frequency of 0.01Hz to 10^5Hz.

3. RESULTS AND DISCUSSION

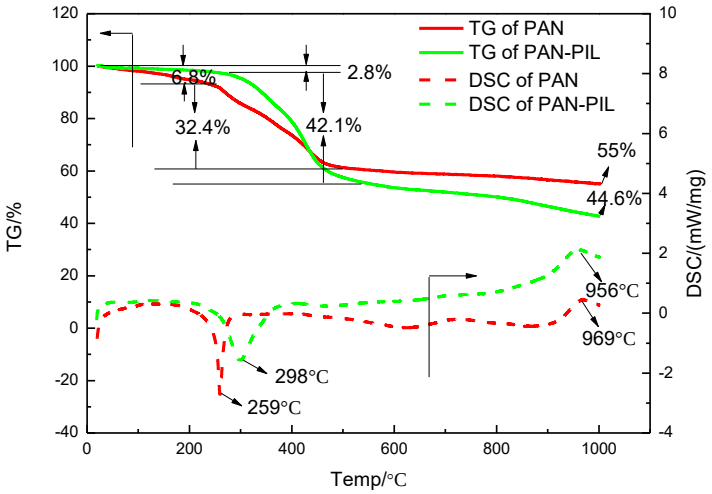

Figure 1. TG/DSC curves of PAN and PAN-PIL

The TG/DSC curves of PAN and PAN-PIL are shown in Figure 1. In the DSC curve of PAN, a sharp exothermic peak appears at 259.6 ºC, indicating that the cyclization reaction and some other exothermic reactions occurred in this stage[46]. The cyclization reaction peak of PAN-PIL becomes broader and appears at a higher temperature (298.6℃). This can be attribute to the imidazole rings of [VEIm]BF_4 in the IL comonomer which may inhibit the cyclization reaction. A blunt peak can be observed at 969ºC and 956 ºC in the DSC curve of PAN and PAN-PIL, respectively.

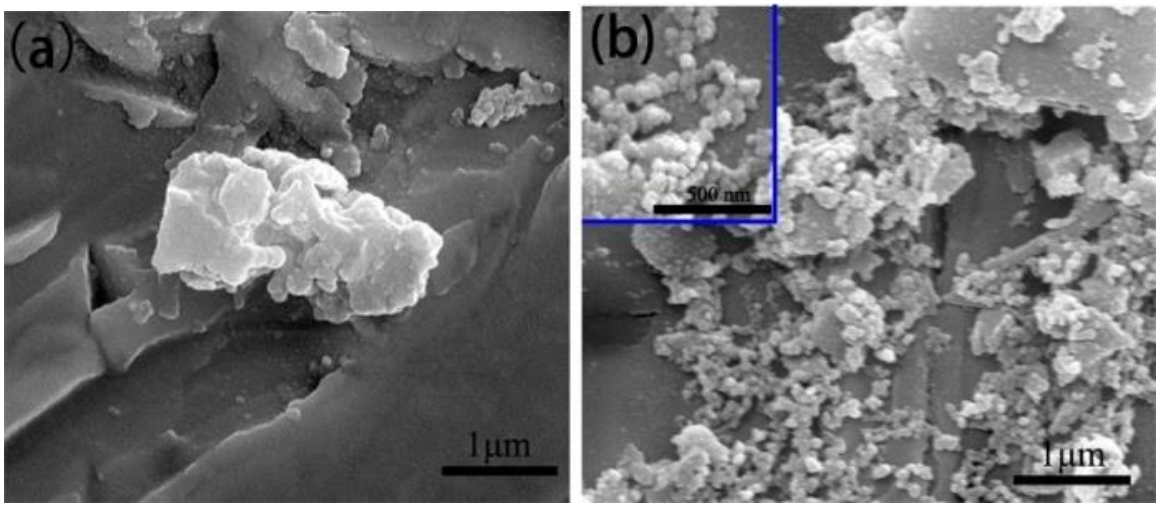

Figure 2. SEM images of CPAN (a) and CPAN-PIL(b)

This peak is induced by the phase transformation of the carbon materials, which is beneficial for a higher irreversible capacity and a lower coulombic efficiency at the first charge/discharge cycle [47].The TG curves of PAN and PAN-PIL can be roughly divided into three segments. As for PAN powders, the first segment is up to 260 ºC. The weight loss is small at this segment As shown in the

TG curves of PAN and PAN-PIL, the major weight loss (>30 wt.%) occurs between 260 ºC to 475 ºC, which can be attributed to the dehydrogenation of PAN and correspond to the DSC exothermic peak at 259.6 ºC. When the temperature is further increased above 475 ºC, PAN-PIL shows more weight loss than PAN because more unstable carbon species are introduced during the doping process of PAN-PIL[48].

The SEM images of CPAN and CPAN-PIL samples are shown Figure 2. The CPAN material appears in walnut kernel structure with a length of ~2μm. While CPAN-PIL material exists in spherical particles with a diameter of 50 nm. The reduced particle size is beneficial for the delivery of lithium ions and is likely caused by the introduction of [VEIm]BF_4 during the polymerization process.

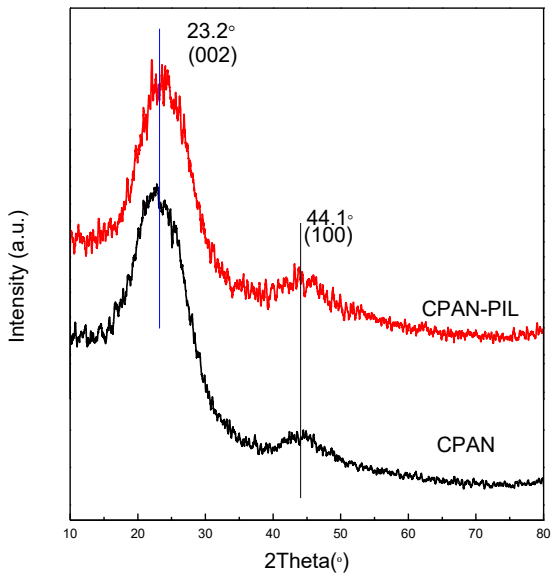

Figure 3. XRD pattern of CPAN and CPAN-PIL

As shown in Figure 3, CPAN and CPAN-PIL samples show similar XRD patterns. Two broad peaks located at 23.2º and 43º correspond to the diffraction of the (002) and (100) crystal planes of carbon, respectively. These broad peaks of CPAN and CPAN-PIL indicate a amorphous carbon structure[10]. The disorder characteristics of amorphous carbon can facilitate the insertion and extraction of lithium ions [49].

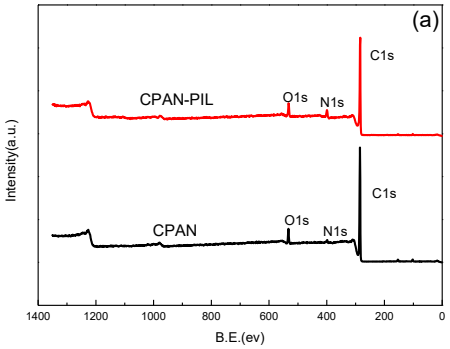

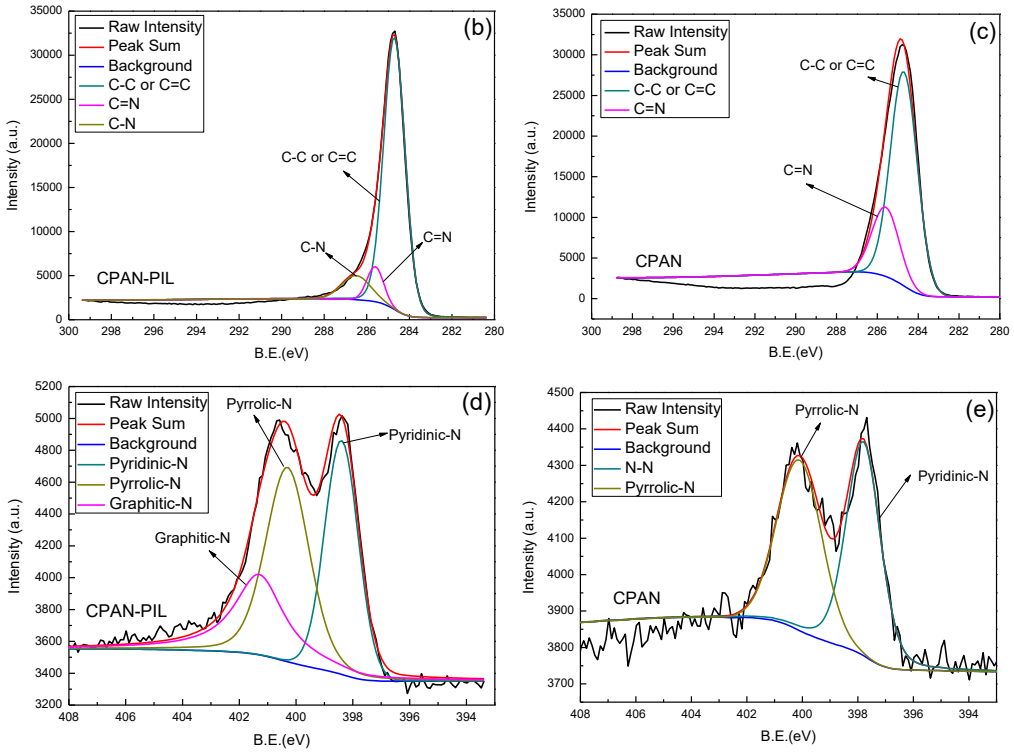

Figure 4. XPS survey spectra of CPAN and CPAN-PIL(a); C 1s of CPAN-PIL(b); C 1s of CPAN(c); N 1s of CPAN-PIL(d); N 1s of CPAN(e).

Moreover, by using the Scherrer formula, the interlayer spacing of the d_{002} plane of CPAN and CPAN-PIL is calculated as 0.38 nm, which is larger than that of graphite (0.34nm). The larger interlayer spacing could also contribute to the intercalation and deintercalation of lithium ions [50].

Table 1. Atomic ratio of relative nitrogen species for CPAN and CPAN-PIL

Samples	N content (at%)	pyridinic nitrogen (at%)	pyrrolic nitrogen (at%)	graphitic nitrogen (at%)
CPAN	2.32	1.20	1.12	0
CPAN-PIL	6.80	2.04	2.75	2.01

The XPS analysis of CPAN and CPAN-PIL is used to determine the elements binding state and the nitrogen content on the surface region (Figure.4a). The XPS spectra of CPAN and CPAN-PIL both display three peaks at 285 eV, 400 eV and 532 eV, corresponding to C 1s, N 1s, and O 1s, respectively [12]. The N 1s peak of CPAN-PIL is obviously stronger than that of CPAN, indicating a higher nitrogen content in CPAN-PIL material. The C 1s spectra of CPAN-PIL and CPAN are shown in Figure 4b and 4c, respectively. Both the C 1s spectrum of CPAN-PIL and CPAN exhibit the deconvoluted peak for C-C or C=C (284.7 eV) and C=N (285.6 eV).[51]. A new peak at 286.5eV raises in the spectra of CPAN-PIL. This peak stems from the C-N group, indicating that new nitrogen

species are introduced onto the carbon frame when IL is used as carbon source. [28].. The N 1s spectra of CPAN-PIL and CPAN are shown in Figure 4d and 4e. The N 1s spectrum of CPAN-PIL can be deconvoluted into three peaks at 398.4 eV, 400.3 eV and 401.3 eV, corresponding to pyridinic-N, pyrrolic-N and graphitic-N, respectively[52]. While no graphitic-N peak is found in the spectrum of CPAN, indicating no C-N is formed; and this is in accordance with the results of Fig. 4b and 4c. To further investigate the effects of IL on the N-doping of carbon materials, the relative atomic ratio of nitrogen species in CPAN and CPAN-PIL are listed in Table 1 according to the fitting results. The N content of CPAN-PIL is 2.9 time of the N content of CPAN. The graphitic-N group only exists in CPAN-PIL and contributes ~30% of the total N content of CPAN-PIL. The p_z-orbital of graphitic-N is occupied by two of the lone pair electrons of the three bonded sp^2 carbon atoms. This nitrogen atom can provide excess electrons in the delocalized π-system, which is favorable for forming an electron-rich structure [29]. Therefore, the electrical conductivity of CPAN-PIL is higher than that of CPAN. The pyridinic-N and pyrrolic-N contents of CPAN-PIL are much higher than those of CPAN as well. On the one hand, the pyridinic-N is more likely to form active sites, resulting in outstanding features near the Fermi level[25]. The pyridinic-N could also take part in the pseudo-capacitive redox reactions of lithium ions[53]. On the other hand, the pyrrolic-N can provide two electrons to the π system and form electrochemically active sites which can improve the capacity of amorphous carbon as LIBs anode materials[54]. Therefore, the high pyridinic-N and pyrrolic-N contents in CPAN-PIL can improve the transmission of lithium ions.

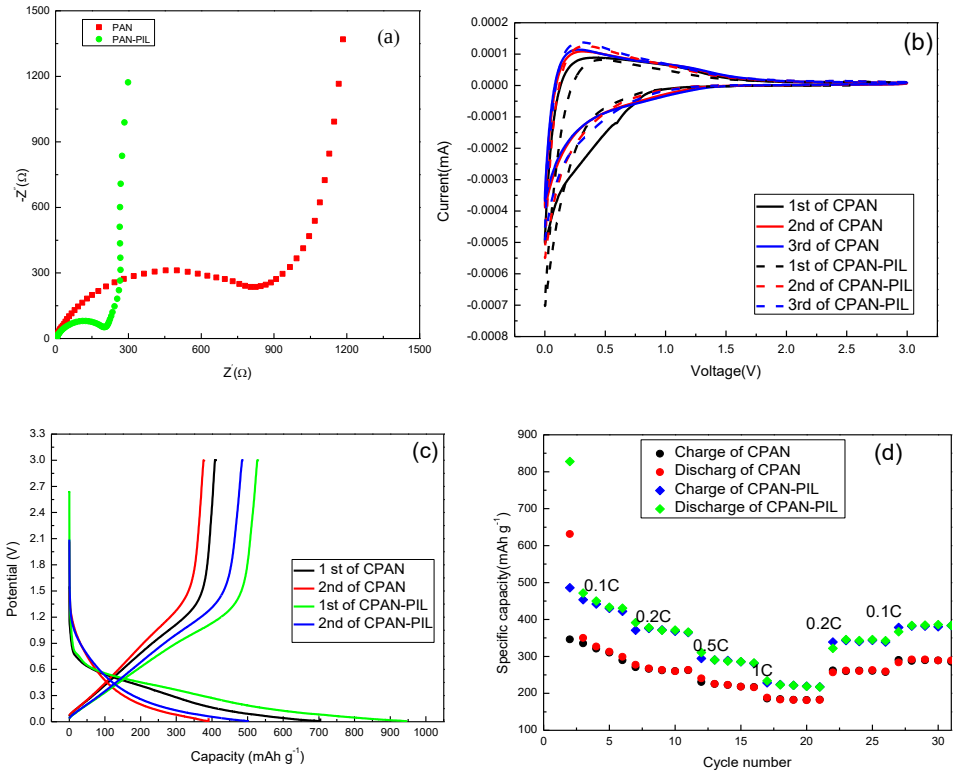

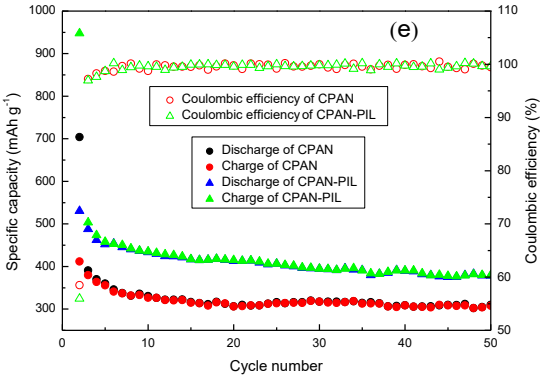

Figure 5. Nyquist plots of the CPAN and CPAN-PIL materials over the frequency range 100 kHz to 0.01 Hz (a); CV curves of the CPAN and CPAN-PIL materials (b); Initial two discharge/charge curves of the CPAN and CPAN-PIL at 0.1C (c); rate capability of the CPAN and CPAN-PIL (d); Specific capacity and coulombic efficiency of the CPAN and CPAN-PIL materials for 50 cycles at 0.1 C (e).

Table 2. Comparison of electrochemical properties of N-doped carbonaceous material used in LIBs

Sample	Carbon source	1st cycle reversible capacity (mA h g^{-1})	Cycle number	Capacity (mAh g^{-1})	Coulombic efficiency after 50th cycles %	Ref.
PAN-CNFs-1000	PAN	410±5	50	280±5	97	[55]
CNFs	PAN	370±5	50	310±5	-	[56]
CC	polyaniline	490	20	272	-	[57]
PAN-HCS-800	PAN	423	100	350	98	[26]
NDC	[BMIm]N(CN)$_2$	420	50	243.6	99	[45]
CPAN	PAN	407	50	309	99	Our
CPAN-PIL	PAN-PIL	526	50	381	99	work

Figure 5a exhibits the Nyquist plots of CPAN and CPAN-PIL from 10^{-2} Hz to10^{5} Hz. The CPAN-PIL shows a much lower charge transfer resistance than the CPAN, indicating higher intercalation/deintercalation ability of lithium ions [50]. This reduced charge transfer resistance is owning to the high nitrogen content in CPAN-PIL and, especially, the graphitic-N group, which lead to a higher charge transfer speed on the electrode/electrolyte interface and, therefore, a higher diffusion rate of lithium ions into carbon materials. The CV curves of CPAN and CPAN-PIL, seen in Figure 5b, shows the typical characteristics of carbonaceous anode materials[50]. A cathodic peak at 0.3~ 0.8 V appears in the first cycle and disappears in the subsequent cycles, indicating the formation of SEI in the first cycle. The CPAN-PIL material exhibits a higher current density than CPAN in all the three cycles. This is because of the high pyridinic-N and pyrrolic-N contents that lead to more active sites and sequentially an enhanced the current density and lithium ion storage capability[31, 54].

Figure 5c shows the first two discharge/charge curves of the CPAN and CPAN-PIL at 0.1C. An obvious inflection point appears in the first discharge cycle and disappears in the second cycle, indicating the formation of a stable SEI film on the electrode, which is in accordance with the results of CV curves[58]. The rate performances of CPAN and CPAN-PIL at the 0.1C, 0.2C, 0.5C and 1C current density are shown in Figure 5d. The specific capacity of CPAN-PIL is obviously higher than that of the CPAN, suggesting the graphitic-N and the high nitrogen content in the CPAN-PIL material is beneficial for the enhancement of specific capacity of CPAN-PIL.

As shown in the Figure 5e, the capacities of CPAN and CPAN-PIL can maintain 309 mAh g^{-1} and 381 mAh g^{-1} after 50 cycles at 0.1C, respectively. These results can be attributed to the disordered structure and defects caused by graphitic-N of CPAN-PIL. It is advanced for the emergence of active sites and enhanced the electrical conductibility of CPAN-PIL. By comparison from Table 2, it is apparent that the CPAN-PIL possessed much higher 1^{st} cycle reversible capacity than other similar materials. Besides, the stable and reversible capacity after 50^{th} cycles of CPAN-PIL also superior to other similar materials, indicating that the ILs play an extremely vital role to enhance the electrochemical performance of carbonaceous anode materials for LIBs.

4. CONCLUSIONS

CPAN-PIL was successfully synthesized using acrylonitrile and [VEIm]BF_4 as monomers by soap-free emulsion copolymerization, followed by carbonation in N_2 atmosphere. The ionic liquid effectively increased the nitrogen content and successfully introduced graphitic-N to CPAN-PIL material. The graphitic-N and high nitrogen content in CPAN-PIL material greatly reduced the charge transfer resistance and increased the active sites of carbon material, improving the capacity, cycle stability and rate performance. Therefore, the incorporation of ionic liquid with acrylonitrile as carbon source is a facile way to enhance the nitrogen content and enrich the doped nitrogen species.

ACKNOWLEDGEMENT
The project was supported by the National Natural Science Foundation of China (grant No. 51364024, 51404124), Natural Science Foundation of Gansu Province (grant No. 1506RJZA100), the Foundation for Innovation Groups of Basic Research in Gansu Province (No. 1606RJIA322).

CONFLICTS OF INTEREST STATEMENT
The authors certify that they have NO affiliations with or involvement in any organization or entity with any financial interest (such as honoraria; educational grants; participation in speakers' bureaus; membership, employment, consultancies, stock ownership, or other equity interest; and expert testimony or patent-licensing arrangements), or non-financial interest (such as personal or professional relationships, affiliations, knowledge or beliefs) in the subject matter or materials discussed in this manuscript.

References

1. Y. Xiao, C. Hu, M. Cao, *Chemistry, an Asian journal*, 9 (2014)351.

2. J. Zhu, C. Chen, Y. Lu, Y. Ge, H. Jiang, K. Fu, X. Zhang, *Carbon*, 94 (2015)189.
3. M.-Y. Li, C.-L. Liu, M.-R. Shi, W.-S. Dong, *Electrochim Acta*, 56 (2011)3023.
4. A.M. Haregewoin, A.S. Wotango, B.-J. Hwang, *Energy Environ. Sci.*, 9 (2016)1955.
5. X. Liu, Y. Wu, Z. Yang, F. Pan, X. Zhong, J. Wang, L. Gu, Y. Yu, *J Power Sources*, 293 (2015)799.
6. Y. Li, X. Lv, J. Lu, J. Li, *The Journal of Physical Chemistry C*, 114 (2010)21770.
7. Y. Zhang, Y. Wang, Y. Meng, G. Tan, Y. Guo, D. Xiao, *RSC Adv.*, 6 (2016)98434.
8. K. Jost, C.R. Perez, J.K. McDonough, V. Presser, M. Heon, G. Dion, Y. Gogotsi, *Energ Environ Sci*, 4 (2011)5060.
9. H.-g. Wang, Y. Wang, Y. Li, Y. Wan, Q. Duan, *Carbon*, 82 (2015)116.
10. C. Shen, C. Zhao, F. Xin, C. Cao, W.-Q. Han, *Electrochim Acta*, 180 (2015)852.
11. W. Cheng, F. Rechberger, D. Primc, M. Niederberger, *Nanoscale*, 7 (2015)13898.
12. W. Guo, X. Li, J. Xu, H.K. Liu, J. Ma, S.X. Dou, *Electrochim Acta*, 188 (2016)414.
13. B. Wu, T. Liu, Q. Xia, X. Wu, *Journal of the Electrochemical Society*, 160 (2013)A1720.
14. X. Yue, W. Sun, J. Zhang, F. Wang, Y. Yang, C. Lu, Z. Wang, D. Rooney, K. Sun, *Journal of Power Sources*, 331 (2016)10.
15. F.-D. Han, Y.-J. Bai, R. Liu, B. Yao, Y.-X. Qi, N. Lun, J.-X. Zhang, *Advanced Energy Materials*, 1 (2011)798.
16. T. Nakajima, *Solid State Sciences*, 9 (2007)777.
17. N. Imanishi, Y. Ono, K. Hanai, R. Uchiyama, Y. Liu, A. Hirano, Y. Takeda, O. Yamamoto, *J Power Sources*, 178 (2008)744.
18. J. Ye, Z. Yu, W. Chen, Q. Chen, S. Xu, R. Liu, *Carbon*, 107 (2016)711.
19. Q. Tian, Y. Tian, Z. Zhang, L. Yang, S.-i. Hirano, *Carbon*, 95 (2015)20.
20. J.G. Kim, F. Liu, C.-W. Lee, Y.-S. Lee, J.S. Im, *Solid State Sciences*, 34 (2014)38.
21. Y. Sun, G. Ning, C. Qi, J. Li, X. Ma, C. Xu, Y. Li, X. Zhang, J. Gao, *Electrochim Acta*, 190 (2016)141.
22. J. Wang, Z. Yang, F. Pan, X. Zhong, X. Liu, L. Gu, Y. Yu, *RSC Adv.*, 5 (2015)55136.
23. J. Qiu, Z. Yang, Y. Li, *J. Mater. Chem. A*, 3 (2015)24245.
24. C. Qian, P. Guo, X. Zhang, R. Zhao, Q. Wu, L. Huan, X. Shen, M. Chen, *RSC Adv.*, 6 (2016)93519.
25. T.M. Czerw R, Charlier J C, et al, *Nano Lett*, 1 (2001)457.
26. J. Jin, Z.-q. Shi, C.-y. Wang, *Solid State Ionics*, 261 (2014)5.
27. S.S. Balaji, M. Sathish, *RSC Adv.*, 4 (2014)52256.
28. J.P. Paraknowitsch, A. Thomas, M. Antonietti, *J Mater Chem*, 20 (2010)6746.
29. M.-G. Jeong, M. Islam, H.L. Du, Y.-S. Lee, H.-H. Sun, W. Choi, J.K. Lee, K.Y. Chung, H.-G. Jung, *Electrochim Acta*, 209 (2016)299.
30. P. Hao, Z. Zhao, Y. Leng, J. Tian, Y. Sang, R.I. Boughton, C.P. Wong, H. Liu, B. Yang, *Nano Energy*, 15 (2015)9.
31. Z. Ling, C. Yu, X. Fan, S. Liu, J. Yang, M. Zhang, G. Wang, N. Xiao, J. Qiu, *Nanotechnology*, 26 (2015)374003.
32. V. Selvamani, R. Ravikumar, V. Suryanarayanan, D. Velayutham, S. Gopukumar, *Electrochim Acta*, 190 (2016)337.
33. J. Ou, L. Yang, Z. Zhang, X. Xi, *J Power Sources*, 333 (2016)193.
34. X. Liu, J. Zhang, S. Guo, N. Pinna, *J. Mater. Chem. A*, 4 (2016)1423.
35. Q.-S. Yang, Z.-Y. Sui, Y.-W. Liu, B.-H. Han, *Industrial & Engineering Chemistry Research*, 55 (2016)6384.
36. C. Hu, Y. Xiao, Y. Zhao, N. Chen, Z. Zhang, M. Cao, L. Qu, *Nanoscale*, 5 (2013)2726.
37. H. Mi, Y. Li, P. Zhu, X. Chai, L. Sun, H. Zhuo, Q. Zhang, C. He, J. Liu, *J Mater Chem A*, 2 (2014)11254.
38. Y. Liu, X. Zhao, G.S. Chauhan, J.-H. Ahn, *Appl Surf Sci*, 380 (2016)151.
39. C.a. Cao, X. Zhuang, Y. Su, Y. Zhang, F. Zhang, D. Wu, X. Feng, *Polym. Chem.*, 5 (2014)2057.

40. K.T. Cho, S.B. Lee, J.W. Lee, *The Journal of Physical Chemistry C*, 118 (2014)9357.
41. A. Piotrowska, K. Kierzek, J. Machnikowski, *Journal of Chemistry*, 2015 (2015)1.
42. H.-P. Steinrück, P. Wasserscheid, *Catalysis Letters*, 145 (2014)380.
43. J. Balach, H. Wu, F. Polzer, H. Kirmse, Q. Zhao, Z. Wei, J. Yuan, *RSC Advances*, 3 (2013)7979.
44. Q. Zhao, T.P. Fellinger, M. Antonietti, J. Yuan, *Macromolecular rapid communications*, 33 (2012)1149.
45. Y. Meng, (2016)9881.
46. E. Cipriani, M. Zanetti, P. Bracco, V. Brunella, M.P. Luda, L. Costa, *Polymer Degradation and Stability*, 123 (2016)178.
47. H. Zhao, Q. Wang, Y. Deng, Q. Shi, Y. Qian, B. Wang, L. Lü, X. Qiu, *RSC Adv.*, 6 (2016)77143.
48. H. Bi, Z. Liu, F. Xu, Y. Tang, T. Lin, F. Huang, *J. Mater. Chem. A*, 4 (2016)11762.
49. J. Ou, L. Yang, X. Xi, *Chinese Journal of Chemistry*, 34 (2016)727.
50. J. Ou, L. Yang, Y. Zhang, L. Chen, Y. Guo, D. Xiao, *Chinese Journal of Chemistry*, 33 (2015)1293.
51. X. Wu, X. Yu, Z. Lin, J. Huang, L. Cao, B. Zhang, Y. Zhan, H. Meng, Y. Zhu, Y. Zhang, *Int J Hydrogen Energ*, 41 (2016)14111.
52. S. Lee, Y.-W. Lee, D.-H. Kwak, J.-Y. Lee, S.-B. Han, J.I. Sohn, K.-W. Park, *Journal of Industrial and Engineering Chemistry*, 43 (2016)170.
53. X. Han, P. Han, J. Yao, S. Zhang, X. Cao, J. Xiong, J. Zhang, G. Cui, *Electrochim Acta*, 196 (2016)603.
54. F. Zheng, Y. Yang, Q. Chen, *Nature Communications*, 5 (2014)5261.
55. J. Jin, Z.-q. Shi, C.-y. Wang, *Electrochimica Acta*, 141 (2014)302.
56. D. Nan, Z.-H. Huang, R. Lv, L. Yang, J.-G. Wang, W. Shen, Y. Lin, X. Yu, L. Ye, H. Sun, F. Kang, *J. Mater. Chem. A*, 2 (2014)19678.
57. X. Xiang, E. Liu, Z. Huang, H. Shen, Y. Tian, C. Xiao, J. Yang, Z. Mao, *Materials Research Bulletin*, 46 (2011)1266.
58. W. Sun, L. Wan, X. Li, X. Zhao, X. Yan, *J. Mater. Chem. A*, 4 (2016)10948.